Highly reflective low-noise etalon-based meta-mirror

Johannes Dickmann[1,*] and Stefanie Kroker[1,2]

[1]Physikalisch-Technische Bundesanstalt, Bundesallee 100, 38116 Braunschweig, Germany
[2]Technische Universität Braunschweig, LENA Laboratory for Emerging Nanometrology, Pockelsstraße 14, 38106 Braunschweig, Germany

(Received 23 July 2018; published 23 October 2018)

We present a concept of a mirror for application in high-reflectivity low-noise instruments such as interferometers. The concept is based on an etalon with a metasurface (meta-etalon) on the front and a conventional multilayer stack on the rear surface. The etalon in combination with the metasurface enables a dedicated spatial weighing of the relevant thermal noise processes and by this a substantial reduction of the overall readout thermal noise. As examples, we illustrate the benefit of the proposed etalon for thermal noise in two applications: the test masses of the Einstein Telescope gravitational wave detector and a single-crystalline cavity for laser frequency stabilization. In the Einstein Telescope, the thermal noise of the etalon even at room temperature outperforms existing concepts for operation temperatures at 10 K. For the laser stabilization cavity, a reduction of the modified Allan deviation of an order of magnitude is predicted.

DOI: 10.1103/PhysRevD.98.082003

I. INTRODUCTION

Thermal noise limits the sensitivity of high-precision measurement devices like interferometric gravitational wave detectors and Fabry-Pérot cavities for the frequency stabilization of lasers [1–5]. Among the noise sources, the Brownian thermal displacement noise of the optical mirror coatings sets the most severe limitation. There are two approaches to reduce thermal noise. The first one addresses the material properties of the optical coatings in stacks of alternating dielectric layer pairs. In this case, the coating thermal noise is mainly determined by the mechanical loss of the coating layers [6–9]. The mechanical loss can be substantially reduced by the use of crystalline coating layers instead of amorphous materials [10–13]. However, thermal noise scales with the coating thickness. Equally, the reflectivity of multilayer stacks increases with the number of layer pairs. For example, coating stacks with a reflectivity of >99.9994% typically requires 30 to 40 quarter-wavelength layers [1,14,15]. This inherent relationship between reflectivity and thermal noise sets a limit to the ultimate noise performance that can be achieved.

The second approach waives the use of alternating layer pairs and therewith the increase of thermal noise with reflectivity. The approach is based on periodic sub-wavelength structures (hereinafter referred to as "metasurfaces") manufactured from a dielectric material with a high refractive index. These structures are designed to provide an optical resonance based on two coupled Bloch modes [16,17]. The modes interfere constructively in the backward direction of the incoming light, enabling a high reflectivity with high spectral and angular tolerance [18,19]. The Bloch modes are localized in a surface layer with a thickness of less than the wavelength of light [17]. With respect to thermal noise, the main advantage of the metasurfaces is that their reflectivity does not scale with their thickness. The minimum thickness is about $\lambda/4n$, where λ is the wavelength of light and n the refractive index of the metasurface. Basic proof-of-principle experiments in interferometry have been performed [20]. However, the maximum reflectivity of 99.8% that was experimentally achieved so far is not sufficient [18] for application in interferometric gravitational wave detectors or laser cavities for frequency stabilization [4,14].

In past years, advances for the rigorous computation of the thermal noise of arbitrarily shaped reflective surfaces were made [21–23]. This lays the foundation for a deeper understanding of the complex interplay of dissipative processes and thermal noise in these systems and prepares the ground for new possibilities in the design of low-noise optical elements.

In this contribution, we present a concept which overcomes limitations in the reflectivity of metasurfaces and simultaneously provides an excellent thermal noise performance. This is realized by combining the optical functions of a conventional multilayer mirror and a metasurface while suppressing the coupling of mechanical fluctuations between each other by the use of an antiresonant etalon (hereinafter referred to as a "meta-etalon"). To illustrate the potential of the proposed concept, we perform a holistic analysis of thermal noise for the low-frequency detector of the Einstein Telescope gravitational wave detector (ET-LF)

*johannes.dickmann@ptb.de

[14] and for crystalline silicon cavities for the frequency stabilization of laser light [4].

The article is organized as follows. In Sec. II we describe the basic layout of the meta-etalon. In Sec. III, we give a brief introduction into the computation of the relevant thermal noise contributions. In Sec. IV, the results of the optical optimization and the noise evaluation are presented and discussed. Computational details and material parameters can be found in the appendixes.

II. ETALON-BASED META-MIRROR

Figure 1 shows a schematic of the etalon-based meta-mirror (meta-etalon). The major fraction of the incident light is reflected by the metasurface at the front. Its intensity reflectivity R_1 is determined by the refractive indices n_g and n_s of the involved materials as well as by the structural parameters W, H, and Λ. Details on the metasurface design will be discussed in detail in Sec. IV A. The residual light being transmitted by the metasurface propagates through the etalon and is reflected by a conventional multilayer stack (refractive indices n_1 and n_2) on the rear surface of the etalon (intensity reflectivity R_2). To achieve a high reflectivity with the whole system, the etalon, forming a two-mirror system, is thermally tuned to antiresonance [24]. For both investigated applications, i.e., the Einstein Telescope (ET) gravitational wave detector and the crystalline silicon cavity for laser frequency stabilization [4,25], we choose the etalon spacer material to be fused silica. The metasurface is made of single-crystalline silicon and the coating stack on the back side of the etalon consists of altering amorphous silica (SiO_2) and tantala (Ta_2O_5) layers. Details on the design can be found in Appendix B. The influence of alternative spacer materials is discussed in Sec. IV. The Einstein Telescope is examined at room temperature, whereas the crystalline silicon cavity with etalon-based meta-mirrors is investigated at 124 K because the linear thermal expansion coefficient vanishes at this temperature, which is beneficial for the frequency stability.

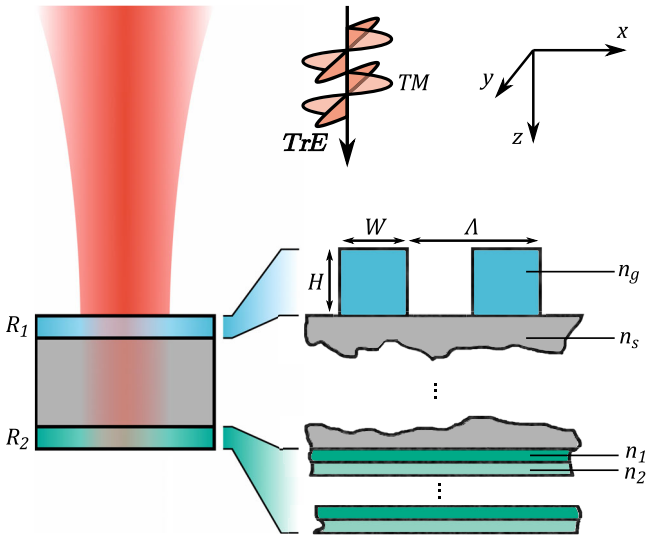

FIG. 1. Schematic of the etalon-based meta-mirror for low thermal noise and high reflectivity. The gray area indicates the etalon spacer, the blue one the nanostructured front surface (metasurface), and the green one the rear surface consisting of a conventional multilayer stack. The intensity reflectivities are R_1 for the metasurface and R_2 for the coating stack. W represents the ridge width, H the ridge height, and Λ the period of the metasurface. The metasurface materials index of refraction is denoted n_g, the substrates n_s, and the altering coatings n_1 and n_2. The electric field vector of the incident light is illustrated for transverse electric (TrE) and transverse magnetic (TM) polarized light.

III. THERMAL NOISE ANALYSIS

In this section, we present basics and assumptions on the thermal noise analysis for the etalon system. First, the Brownian noise resulting from thermally activated local transitions between the minima of asymmetric bistable potentials, associated to quasidegenerate bond states, is studied. It leads to a spatially fluctuating surface. The second source of noise is volume fluctuation of the solid, which leads to spatially fluctuating light paths and thus to a fluctuating phase. This noise type is called thermoelastic (TE) noise. The third noise type—the thermorefractive (TR) noise—results from fluctuations of the refractive index. For each component of the etalon system, i.e., the metasurface at the front, the etalon substrate, and the multilayer stack on the rear surface Brownian, TE and TR noise are investigated. As shown by Evans *et al.*, correlations between TE and TR noise enable a partial compensation of both noise sources summed up to thermo-optic noise [26]. Here, we consider a worst-case scenario without any correlation between the individual noise contributions. This uncorrelated sum of all noise sources provides an upper limit of the overall noise that has to be expected.

We now briefly introduce the physical quantities we use for the discussion of thermal noise. The starting point for both systems, ET and the crystalline silicon cavity, is the determination of the thermal noise displacement power spectral density S in $m^2\ \mathrm{Hz}^{-1}$. From that, the mirror thermal noise of the test masses in ET is calculated as thermal noise displacement spectral density $\sqrt{S}$. As an uncorrelated sum, this quantity reads

$$\sqrt{S} = \left(\sum\nolimits_i S_i\right)^{1/2}. \tag{3.1}$$

The summation includes all noise contributions S_i. To describe the frequency stability of the silicon cavity in dependence of the integration time τ [4] instead of thermal displacement noise, the modified Allan deviation σ_y is determined. To this end, first the thermal noise power spectral density S is converted into a frequency noise spectral density $\tilde{S}$ in $\mathrm{Hz}^2\ \mathrm{Hz}^{-1}$:

$$\tilde{S} = \frac{c^2}{(\lambda L)^2} S. \tag{3.2}$$

Here c is the speed of light in vacuum, λ the wavelength of light, and L the length of the cavity. Again, $\tilde{S}$ contains the uncorrelated sum of all noise contributions of the system. From $\tilde{S}$ the modified Allan deviation at the readout frequency f is computed [27]:

$$\sigma_y(\tau) = \left(\frac{2\lambda^2}{c^2} \int_0^\infty \tilde{S}(f) \frac{\sin^4(\pi\tau f)}{(\pi\tau f)^2} df \right)^{1/2}. \tag{3.3}$$

A. Brownian thermal noise

In this section we outline the computation scheme of Brownian thermal noise for the etalon from first principles [22,28]. The scheme employs Levin's approach of virtual pressures [29] and the ponderomotive pressures of the light field resulting from the Maxwell stress tensor. The starting point is the fluctuation-dissipation theorem (FDT). It relates the dissipated power under the effect of a virtual pressure to the thermal noise of an optical element [29]:

$$S = \frac{2k_B T}{\pi^2 f^2} \frac{W_{\mathrm{diss}}}{F_0^2}, \tag{3.4}$$

where k_B is the Boltzmann constant, T the temperature of the optical element, f the mechanical readout frequency, W_{diss} the dissipated power under the virtual pressure, and F_0 the surface integral of the virtual pressure. The spatial weighing of the virtual pressure is given by the Maxwell stress tensor (in SI units):

$$\sigma_{ij} = \epsilon_0 \epsilon_r E_i E_j + \frac{1}{\mu_0 \mu_r} B_i B_j - \frac{1}{2} \left(\epsilon_0 \epsilon_r E^2 + \frac{1}{\mu_0 \mu_r} B^2 \right) \delta_{ij}. \tag{3.5}$$

The indices i and j denote the spatial coordinate basis, E_i are the components of the electric field, B_i the components of the magnetic field, $\epsilon_0 \epsilon_r$ is the permittivity, $\mu_0 \mu_r$ is the permeability, and δ_{ij} is the Kronecker symbol. The difference of the stress tensor inside and outside the investigated optical surface leads to the ponderomotive light pressure:

$$\vec{p}(\vec{r}) = \Delta\hat{\sigma}(\vec{r}) \frac{\vec{A}}{A}(\vec{r}). \tag{3.6}$$

The quantity $\Delta\hat{\sigma}$ must be evaluated *directly* at the surface as the difference between the stress tensor components in vacuum and material. $\vec{A}/A$ represents the normalized normal vector on the surface. Generally, this expression is evaluated using the transition conditions for electric and magnetic fields at the surface. For example, if the normal vector of the surface is parallel to the direction i, and the material is not magnetically active, i.e., $\mu_r = 1$, the pressure can be expressed by the continuous field components either inside or outside the material:

$$p_i = \frac{1}{2} \left(\frac{D_i^2}{\epsilon_0} \left(\frac{1}{\epsilon_1} - \frac{1}{\epsilon_2} \right) + \epsilon_0 (E_j^2 + E_k^2)(\epsilon_2 - \epsilon_1) \right), \tag{3.7}$$

with the electric displacement field $D_i = \epsilon_0 \epsilon E$ and the permittivity $\epsilon_0 \epsilon_1$ outside and $\epsilon_0 \epsilon_2$ inside the material. Applying the ponderomotive pressure, modulated by the readout frequency f, on the optical component introduces an elastic deformation energy density $\mathcal{E}_{\mathrm{el}}$ into the component. This leads to a dissipation of energy, proportional to the mechanical loss angle Φ of the material:

$$W_{\mathrm{diss}} = 2\pi f \int_V \Phi \mathcal{E}_{\mathrm{el}} dV. \tag{3.8}$$

With the dissipated energy W_{diss} and Eq. (3.4), Brownian thermal noise can be computed. Equation (3.8) illustrates that thermal noise is affected by the spatial distribution of the mechanical loss *in combination* with the spatial distribution of the electromagnetic fields determining the fluctuation readout. As a rule of thumb, the detrimental effect of mechanical losses on Brownian noise is smaller, the lower the amplitudes of the relevant electromagnetic field components at the surface of the lossy material. That means, to mitigate Brownian thermal noise, it is essential to deliberately shape the spatial distribution of the mechanical losses and, if possible, the distribution of the electromagnetic field. This is the reason why highly reflective metasurfaces made of high refractive index materials can exhibit an extraordinarily low thermal noise [22,23]. In these structures, the electromagnetic field is localized within the volume and the field at the surface is reduced (see Sec. IV A). This leads to a drastically reduced, i.e., optimized, readout of thermal noise. The computation of thermal noise in binary high-reflectivity metasurfaces is discussed in detail in [23].

Brownian thermal noise of plane etalons coated with multilayer mirrors on the front and back surface can be described by the approach investigated in [30,31]. However, in the present case, the periodic metasurface requires us to additionally apply a spatially oscillating pressure to the etalon substrate. The spatial oscillation period is the period of the metasurface. Thus, additionally, the elastic energy due to this oscillation $\mathcal{E}_{\mathrm{osc}}$ must be considered. For this problem, an analytical solution does not exist yet. A comprehensive numerical computation with finite element analysis is challenging, because the spatial oscillating period is much smaller than the whole etalon system (e.g., in the case of ET by a factor of 500 000 smaller), which would inevitably lead to an immense number of vertexes in the finite element simulation. To circumvent this problem, we develop a semianalytical approach. We analytically calculate the deformation energy density induced by the smooth part

of the pressure, which is determined by the shape of the incident light beam. The spatial intensity profile of a Gaussian distributed light beam reads

$$I(r) = I_0 \exp\left(-\frac{r^2}{r_0^2}\right), \tag{3.9}$$

where r is the distance from the center of the beam, measured on the reflective surface. I_0 represents the intensity at the center $r = 0$ and r_0 is the Gaussian beam radius, where the intensity has dropped to $1/eI_0$. Not the total ponderomotive pressure acts on the front surface of the etalon, because a small fraction $1 - R_1$ of the light is transmitted. Therefore, the pressures are scaled with the coefficients e_1 for the front surface and e_2 for the rear surface, respectively. For an etalon tuned to antiresonance, the coefficients can be expressed by [31]

$$e_1 = \frac{\sqrt{R_1}[1 + (1 + n_s)\sqrt{R_1 R_2} + R_2] + \sqrt{R_2}(1 - n_s)}{(1 + \sqrt{R_1 R_2})^2}, \tag{3.10}$$

$$e_2 = \frac{n_s\sqrt{R_2}(1 - R_1)}{(1 + \sqrt{R_1 R_2})^2}. \tag{3.11}$$

Thus, by adjusting the reflectivities of the etalon's front and back side, it is again possible to minimize the thermal noise readout.

The spatially oscillating part of the elastic deformation energy is determined for one single period of the metasurface using COMSOL [32]. The intensity of the incident light is assumed to be constant over the structural period. This is valid if the Gaussian beam diameter is much larger than the period. For ET, the period is about 6700 times smaller than the beam radius and for the silicon cavity it is about 500 times smaller. The numerical result for a single period is then scaled to the whole Gaussian readout following the scheme in [23]. Both contributions to the elastic energy, the smooth and the oscillating, are then summed to provide an upper limit of the overall noise. In the limit of a large substrate size with thickness $h \gg r_0$ and diameter $d \gg r_0$, the etalon thermal noise can be computed by (using [33])

$$S_{\mathrm{B}}^{\mathrm{sub}} = \frac{4k_B T}{\pi f}\left(\mathcal{E}_{\mathrm{osc}} + e_1^2 \frac{1}{2\sqrt{2\pi}} \frac{1 - \nu^2}{r_0 Y}\right)\Phi, \tag{3.12}$$

with the Poisson's ratio of the substrate ν and the Young's modulus Y. Φ is the loss angle of the substrate material.

The third contribution to Brownian noise results from the coating stack at the back side of the etalon. In the far field, at the back side of substrates with thicknesses much larger than the wavelength, any spatial modulation of the light field caused by the metasurface can be neglected. The etalon we consider here has a thickness which is by a factor of 4000 larger than the wavelength of light. Thus, the field distribution has in good approximation a Gaussian profile—both in reflection and in transmission. With this approximation, the coating thermal noise can be calculated with the model by Nakagawa *et al.* [34]. The respective power spectral density now has to be scaled with the factor e_2^2. It reads

$$S_{\mathrm{B}}^{\mathrm{lay}} = e_2^2 \frac{2k_B T}{\pi^2 f} \frac{(1 + \nu)(1 - 2\nu)}{Y} \frac{d}{r_0^2}\Phi, \tag{3.13}$$

where ν is the mean Poisson's ratio and Y the averaged elastic modulus of the layer stack. Φ is the averaged mechanical loss angle of the two coating materials and d represents the total thickness of the layer stack.

B. Thermoelastic noise

A nonlinear component of the thermo-optic noise is the thermoelastic noise. In contrast to conventional mirrors, it turned out not to be negligible in the composition of thermal noise of etalon-based reflectors. However, the TE noise is studied very well for conventional mirrors and etalons [26,31]. The fluctuation-dissipation theorem is applicable to this noise type, as well. The main difference to the computation of Brownian noise is that here the dissipation mechanism is the heat flow caused by local volume fluctuations. In its general form, this dissipated power is [35]

$$W_{\mathrm{diss}} = 2\pi\kappa T\left(\frac{Y\alpha}{(1 - 2\nu)C\rho}\right)^2 \int_h \int_0^R [\nabla\theta]^2 r dr, \tag{3.14}$$

where κ is the thermal conductivity, C is the thermal capacity per unit volume, Y is the Young's modulus, ν is the Poisson's ratio, α is the thermal expansion coefficient, and ρ is the density. The quantity θ is defined as the trace of the strain tensor, which reads in cylindrical coordinates

$$\theta = \epsilon_{rr} + \epsilon_{\phi\phi} + \epsilon_{zz}. \tag{3.15}$$

The thermoelastic noise of the substrate and the multilayer on the rear surface can be computed with the dissipated energy given by Eq. (3.14). In accordance with the work by Heinert *et al.* [21], the metasurface contribution to thermoelastic noise is evaluated numerically by means of rigorous coupled wave analysis (RCWA) [36]. The computation is performed as follows: generally, a temperature change ΔT leads to a relative length change $\delta = \alpha\Delta T$. In the case of small temperature changes $\Delta T \ll T$, this results in a linear change of the reflected lights phase:

$$\delta\varphi = K_{\mathrm{TE}}\delta, \tag{3.16}$$

where K_{TE} is a numerically determined proportional factor. For this computation, the following three contributions must be considered: (i) the geometrical change of the metasurface

ridge's height and width, (ii) the effective movement of the ridges towards the incident light, and (iii) the change of the metasurface period. For more details on the implementation of the numerical analysis, see Appendix A. Thus, the metasurface's contribution to TE noise reads [21]

$$S_{\mathrm{TE}}^{\mathrm{grat}} = \left(\frac{\lambda}{4\pi} K_{\mathrm{TE}} \alpha\right)^2 S_T, \tag{3.17}$$

where S_T represents the noise power of temperature fluctuations introduced in [37]

$$S_T = \frac{k_B T^2}{\pi^{3/2} r_0^2 \sqrt{\rho C \kappa f}}. \tag{3.18}$$

C. Thermorefractive noise

The second component of the thermo-optic noise results from the spatially fluctuating index of refraction in the material crossed by the light field [31]. For the substrate TR noise, the power spectral density reads [31]

$$S_{\mathrm{TR}}^{\mathrm{sub}} = e_2^2 \frac{k_B T^2 \beta \kappa d}{\pi^2 \rho^2 C^2 r_0^4 f^2} \left(1 + \frac{1}{1 + (4\pi/\lambda\sqrt{\kappa/2\pi C\rho f})^4}\right), \tag{3.19}$$

where $\beta = dn/dT$ is the thermo-optic coefficient. Similarly to Brownian noise, also the thermorefractive noise scales with the weighing coefficients e_i. The second term of (3.19) results from the standing wave inside the etalon tuned to antiresonance. For the coating, TR noise follows [31]

$$S_{\mathrm{TR}}^{\mathrm{coat}} = e_2^2 \times \frac{k_B T^2 \beta_{\mathrm{eff}}^2 \lambda_0^2}{\pi^{3/2} \sqrt{\kappa \rho C} r_0^2 \sqrt{f}}, \tag{3.20}$$

with the effective thermo-optic coefficient of [31]

$$\beta_{\mathrm{eff}} = \frac{1}{4} \frac{\beta_1 n_2^2 + \beta_2 n_1^2}{n_1^2 - n_2^2}, \tag{3.21}$$

where the index 1 indicates the quantity of material 1, i.e., fused silica, and the index 2 indicates the material 2 of the multilayer, i.e., tantala. The metasurface contribution to TR noise is again computed using the RCWA code. The computation is performed as follows. A change in the refractive index of the metasurface material Δn changes the phase of the reflected light. For small values $\Delta n \ll n$, the phase change of the reflected light is proportional to this change:

$$\Delta\varphi = K_{\mathrm{TR}} \Delta n, \tag{3.22}$$

with the proportional constant K_{TR}. This constant is evaluated numerically (see Appendix A). Thus, the noise power can be expressed as [21]

$$S_{\mathrm{TR}}^{\mathrm{grat}} = \left(\frac{\lambda}{4\pi} K_{\mathrm{TR}} \beta\right)^2 S_T. \tag{3.23}$$

IV. RESULTS AND DISCUSSION

A. Optical optimization

The optical design of the etalon configuration aims at a maximum reflectivity in combination with low thermal noise. As demonstrated in the previous section, the noise contributions of the front side and back side have to be weighed by the coefficients e_1 and e_2, which, in turn, depend on the front side and back side reflectivities R_1 and R_2. Thus, in the etalon configuration, Brownian and thermo-optic noise are actually coupled, whereby the coupling is dictated by R_1 and R_2. In this section we illustrate the influence of metasurface reflectivity R_1 and the resulting fabrication tolerances on the weighing factors e_1 and e_2. To this end, the overall transmission of the combined etalon system is <6 ppm and we assume a coating stack reflectivity R_2 of 99.9994% as a typical value for reflectivities of high-performance multilayer mirrors [1] (see Table IV).

The structure parameters of the metasurface, a subwavelength binary grating structure with one-dimensional periodicity, are determined by means of RCWA [36] (wavelength 1.55 μm). As discussed in Sec. III A, the use of structures made of a material with high refractive index, e.g., silicon, are promising for low thermal noise. Here, we consider the metasurface to be made of crystalline silicon on a fused silica substrate [silicon on insulator (SOI)]. We investigate transverse-electric polarized (TrE) light because it is beneficial for the noise performance of metasurfaces with one-dimensional periodicity [23]. Structure period, ridge height, and ridge width are optimized to achieve high reflectivities *in combination* with large tolerances for the ridge height and ridge width, which are the critical parameters in the fabrication process. This parameter range is maximized for a period of $\Lambda = 950$ nm. Figure 2 shows the reflectivity R_1 in dependence of the metasurfaces' ridge height and width. The permitted fabrication tolerances for three exemplary reflectivities are in the range of a few tens of nanometers. For binary structures, these tolerances are realistic in terms of technological feasibility [38].[1]

Besides the residual transmission of the metasurface, material absorption in silicon may limit the feasible reflectivity. We evaluated the influence of the silicon material absorption on the intensity absorption of the metasurface by means of RCWA. The measured absorption coefficient of silicon is as low as 5×10^{-6}/cm [39]. To account for a potentially enhanced absorption due to the large surface-to-volume ratio of the metasurface, as a worst-case scenario, we assume the absorption coefficient to be enhanced by a factor of 100 [40]. In this case, the intensity absorption of the metasurface is still smaller than 10^{-10} and thus can be neglected.

[1]The metasurfaces can be fabricated, e.g., via electron beam lithography and subsequent reactive ion etching.

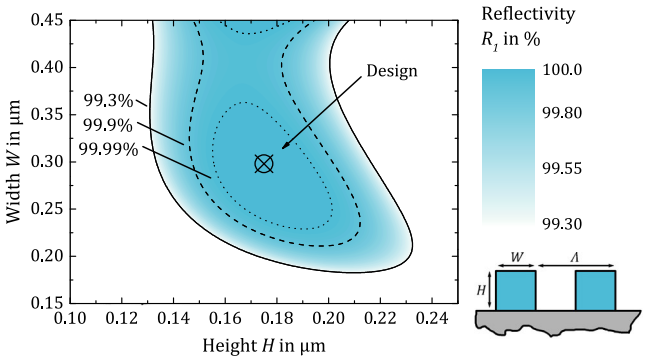

FIG. 2. Contour plot of the metasurface reflectivity in dependence of structure height H and width W. The isolines indicate the parameter spaces for reflectivities of 99.3%, 99.9%, and 99.99%, respectively.

A typical spatial distribution of the electromagnetic energy density in such a high-reflectivity structure is illustrated in Fig. 3. The energy density is concentrated within the volume of the silicon ridges and only slightly enhanced at the surface of the ridges, which leads to the aforementioned minimized readout of thermal noise.

Table I shows the weighing coefficients e_1 and e_2 for the three different values of R_1. The metasurface's contribution to Brownian thermal noise (scaling with e_1^2) does not significantly change with R_1. That means R_1 is not a critical parameter for Brownian thermal noise. In contrast, the contributions of thermorefractive noise scaling with e_2^2 [compare Eqs. (3.19) and (3.20)] change by a factor of more than 5000. Hence, the etalon allows the tuning of the

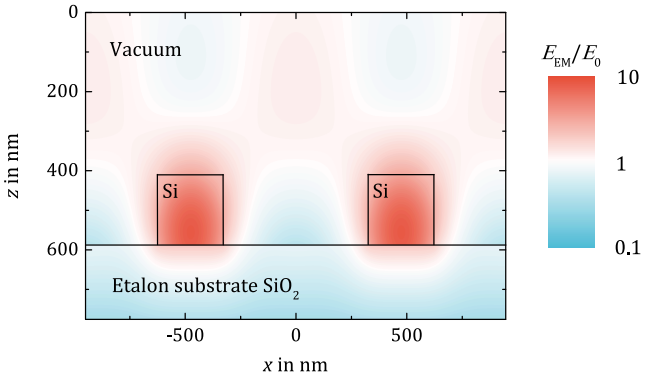

FIG. 3. Contour plot of the electromagnetic field energy density in the silicon metasurface of the etalon (metasurface parameters listed in Table IV). The energy density is normalized to the incident energy density. The plot shows the spatial distribution in the $x-z$ plane of two unit cells of the structure. The energy density is concentrated in the silicon, but it is only slightly enhanced at the surface of the silicon. In addition, the energy density in the area between the ridges is reduced and inside the etalon substrate the energy density decreases rapidly. This spatially modulated light energy density distribution leads to the minimized readout of thermal noise.

TABLE I. Overview of the optical etalon parameters e_1 and e_2 for different reflectivities of the metasurface R_1.

Metasurface reflectivity R_1	Coating reflectivity R_2	e_1	e_2
99.3%	99.999 4%	0.997 454	0.000 790
99.9%	99.999 4%	0.999 637	0.000 113
99.99%	99.999 4%	0.999 964	0.000 011

different noise contributions and provides an additional degree of freedom for low-noise high-reflectivity mirrors.

B. Einstein Telescope

The design parameters for the end mirrors, i.e., the end test masses, of the Einstein Telescope are summarized in Table II. The material parameters for the computation are listed in Table V. ET is a future interferometric gravitational wave detector and its low-frequency part (ET-LF) will be optimized for gravitational wave signals with frequencies of about 1 to 250 Hz [14]. To mitigate thermal noise, the mirrors of ET-LF are planned to operate at cryogenic temperatures of about 10 K. The cryogenic operation of ET will entail immense technical effort. The proposed meta-etalon can achieve the cryogenic thermal noise performance of amorphous multilayer mirrors even at room temperature. To illustrate that, we compare the thermal noise of multilayer mirrors at a temperature of 10 K to the meta-etalon at room temperature. All other parameters, such as laser wavelength, arm length, and laser power, are the same as in the cryogenic design [14]. Figure 4 shows the results of the analysis for all thermal noise contributions using a metasurface reflectivity of $R_1 = 99.3\%$.

In the entire detection bandwidth from 1 to 250 Hz, thermal noise of the etalon is about 10% smaller than the sensitivity of ET-LF at 10 K. Brownian thermal noise of the etalon substrate dominates all other contributions. This means that a further improvement of the metasurface reflectivity R_1 is not beneficial, as it only affects thermo-optic (i.e., TE and TR) noise. Compared to mirrors based on stand-alone high-reflectivity silicon metasurfaces as discussed for ET-LF [18,21,41], meta-etalons enable another improvement of the overall thermal noise. This is thanks to the reduction of Brownian thermal noise as the dominant noise source at the expense of thermo-optic noise. The dominance of substrate Brownian noise is additionally remarkable because conventional multilayer mirrors are limited by the Brownian noise of the coating stack. There are still possibilities for further improvement, especially by using crystalline substrate materials like sapphire or silicon.

C. Single-crystalline silicon cavity

The cavities under investigation are made of single-crystalline silicon with a length of 21 cm (geometrical parameters are listed in Table III). A typical application temperature is the temperature of the zero in the thermal

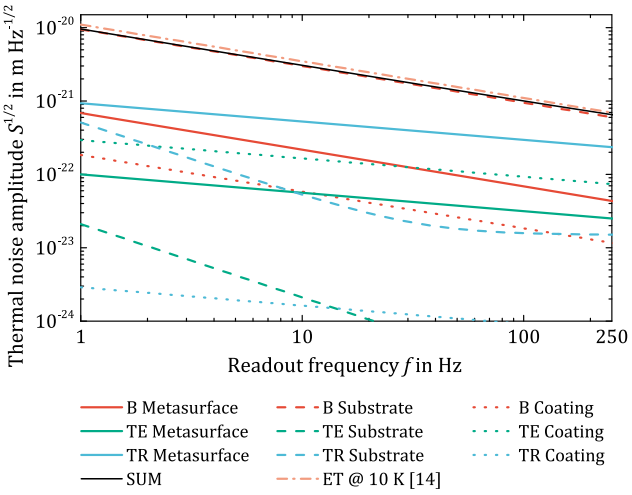

FIG. 4. Room temperature thermal noise amplitudes of all meta-etalon components (metasurface, substrate, and rear surface coating) for ET-LF versus the mechanical readout frequency. A residual transmission of 0.7% of the metasurface was assumed. The plot shows Brownian (B), thermoelastic (TE), and thermorefractive (TR) noise for each component. The black line indicates the uncorrelated sum over all contributions. The current design of ET at a temperature of 10 K (with state-of-the-art amorphous multilayer mirrors) is shown by the dashed-dotted line in magenta color.

expansion coefficient of silicon at 124 K (material parameters for the computation are listed in Table VI).

Figure 5 shows the noise contributions for a silicon cavity with two meta-etalon mirrors for mechanical frequencies from 10^{-3} to 10^{7} Hz. At frequencies >1 Hz, Brownian substrate noise dominates. At low frequencies <0.1 Hz, the thermorefractive noise of the substrate makes the main contribution. By changing the residual transmission of the metasurface, the TR contribution of the substrate can be tuned in the following way. For smaller residual metasurface transmissions, the readout of the TR substrate noise decreases with the weighing coefficient e_2^2 (compare Sec. IV A), because the intensity circulating in the etalon is reduced. Instead, as already mentioned above, the substrate Brownian noise does not change significantly with a higher reflectivity of the metasurface, because the effective ponderomotive pressure on the front surface is almost independent of R_1. Figure 6 shows the influence of R_1 on the thermal noise as a modified Allan deviation for a silicon cavity with two meta-etalons with $R_1 = 99.3\%$, 99.9%, and 99.99%. For comparison, the measured stabilities of the silicon cavities at Physikalisch-Technische Bundesanstalt (Si1-Si3) are illustrated.

In general, the frequency stability of the meta-etalon-based cavity is limited by Brownian substrate noise for small integration times and by the substrate TR noise for large integration times. The integration time, at which TR noise becomes dominant, is crucially affected by the reflectivity R_1 of the metasurface. The higher R_1 is, the larger the integration time until which the Brownian noise floor defines the stability. For $R_1 = 99.99\%$, the stability limitation of the meta-etalon-based cavity in terms of thermal noise is about a factor of 10 better than for state-of-the-art cavities. The fabrication tolerances of about 15 nm for the structure's ridge width and height (see Fig. 2) are in reach with available technology. A further improvement of the frequency stability by a factor of up to 100 can be obtained with crystalline materials like sapphire or silicon as the etalon substrate or lower temperatures (e.g., a few K).

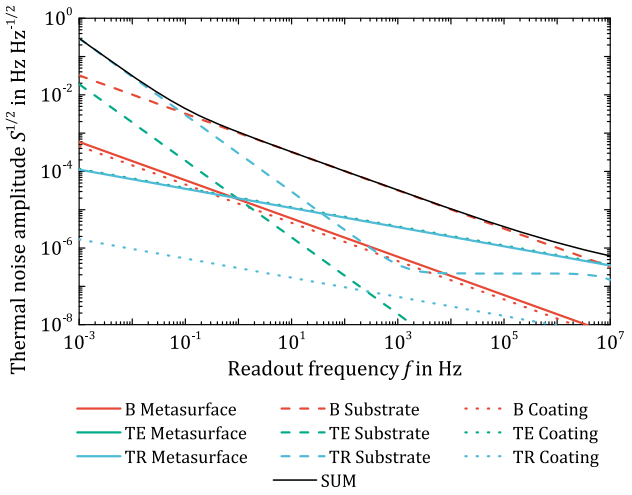

FIG. 5. Thermal noise amplitudes of all meta-etalon components (metasurface, substrate, and rear surface coating) of the Fabry-Pérot cavity versus the mechanical readout frequency. A residual transmission of 0.7% of the metasurface was assumed. The diagram shows the Brownian (B), thermoelastic (TE), and thermorefractive (TR) noise for each component. The black line indicates the uncorrelated sum over all contributions. The TE coating and TE metasurface noise are smaller than 10^{-8} Hz Hz$^{-1/2}$.

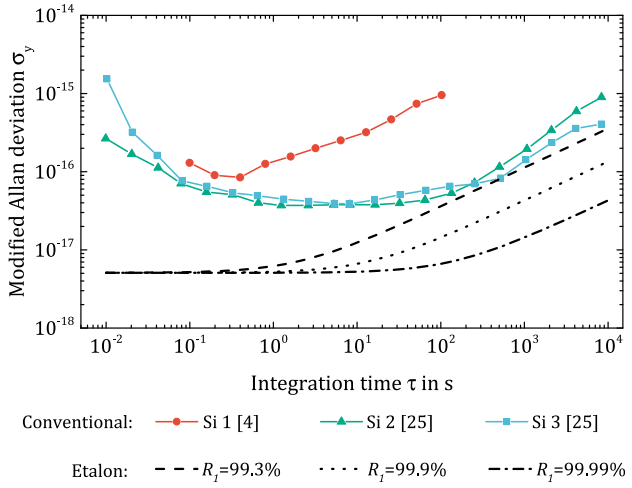

FIG. 6. Modified Allan deviation versus integration time for single-crystalline silicon Fabry-Pérot cavities with different mirrors. Si1-Si3 are cavities with conventional multilayer mirrors. The black lines indicate the cavity performance with meta-etalons as mirrors for different metasurface reflectivities R_1.

V. CONCLUSION

In this paper we presented a concept for a low-noise highly reflective mirror based on an antiresonant meta-etalon with a metasurface at the front surface and a conventional amorphous multilayer mirror at the back surface. To reach a high reflectivity, the meta-etalon must be tuned to optical antiresonance. This can be done by thermal stabilization. Generally, the tolerances for keeping an optical resonator in antiresonance are large, which is promising for temperature stabilization. In comparison to low-noise metasurfaces with ultrahigh reflectivities as stand-alone mirrors in high-finesse cavities, the two-mirror system of the meta-etalon relaxes fabrication tolerances and thus technological challenges in the realization.

We demonstrated as an example the benefit of the meta-etalon based on a fused silica substrate for two devices. For the ET, we demonstrated that the etalon achieves the cryogenic noise performance of conventional multilayer mirrors even at room temperature. In crystalline silicon resonators, the meta-etalon enables a thermal noise reduction by a factor of 10 with fused silica as substrate material.

The meta-etalon is limited by substrate Brownian noise, which can be further reduced by a factor of up to 100 using crystalline substrate materials like sapphire or silicon. In contrast, conventional mirrors are limited by the Brownian thermal noise of the high-reflectivity coating. In the meta-etalon, thermal noise of the metasurface *and* coating thermal noise are both smaller than substrate Brownian noise by a factor of about 10^4 and thus negligible. Due to the dedicated spatial weighing of the dissipation processes in the meta-etalon, the use of amorphous coating materials with high mechanical losses of about 10^{-4} does not compromise the noise performance of the mirror. This can be considered as a paradigm change for the design and optimization of high-precision sensing devices, providing new degrees of freedom to optimal optical performance with minimum thermal noise.

ACKNOWLEDGMENTS

The authors thank T. Legero and U. Sterr for the helpful exchange concerning laser stabilization. Furthermore, J. D. acknowledges A. J. Berghäuser for the linguistic support.

APPENDIX A: SUPPLEMENTAL MATERIAL ON THERMAL NOISE COMPUTATION

In this appendix we provide supplemental information in the computation of the different types of thermal noise.

1. Brownian noise

a. Brownian noise: Metasurface

The computation of Brownian thermal noise of binary metasurface mirrors is comprehensively discussed in [23]. The computations are based on finite element simulations with COMSOL Multiphysics [32] and they are performed over one period of the metasurface structure using Floquet boundary conditions $\vec{k} = 2\pi/\Lambda \vec{e}_x$, where $\vec{e}_x$ represents the unit vector in the x direction (compare Fig. 1 in Sec. I). The simulation in COMSOL is set up as a two-dimensional analysis in the x–z plane.

In the first step, the electromagnetic field in the structure is computed with a spatially constant energy density of the illuminating light field. The power of the incident light is set to $d\tilde{P}/dy = 1$ W/m (in the y direction). Then, the resulting Maxwell stress tensor is applied to the interfaces of the structure. This introduces an elastic deformation energy of density $d\tilde{E}/dy$ to the metasurface ridges:

$$\frac{d\tilde{E}}{dy} = 5.324 \times 10^{-30}\ \frac{\mathrm{J}}{\mathrm{m}}. \tag{A1}$$

Following the scheme in [23], we evaluate thermal noise for the illumination by the entire Gaussian beam:

$$S_{\mathrm{B}}^{(1)} = \frac{2k_B T}{\pi^2 f}\frac{\Lambda}{r_0^2}\frac{\mathrm{d}\tilde{E}}{\mathrm{d}y}\left(\frac{2}{c}\frac{\mathrm{d}\tilde{P}}{\mathrm{d}y}\right)^{-2}\Phi. \tag{A2}$$

b. Brownian noise: Substrate

As discussed in Sec. III, the substrate Brownian noise consists of two contributions: a smooth contribution due to the Gaussian beam and a spatially oscillating contribution originating from the periodic metasurface. The smooth part is evaluated analytically using Eq. (3.12) in Sec. III. The second part is again calculated using a two-dimensional COMSOL simulation. The resulting linear energy density reads

$$\frac{d\tilde{E}}{dy} = 2.122 \times 10^{-30}\ \frac{\mathrm{J}}{\mathrm{m}}, \tag{A3}$$

which is about 4 orders of magnitude smaller than the smooth Gaussian part.

c. Brownian noise: Coating stack

The Brownian noise of the coating stack is evaluated analytically using Eq. (3.13) for a coating stack of 18 $\lambda/4$ doublets of silica/tantala.

2. Thermoelastic noise

Substrate and coating thermoelastic noise are computed analytically following Sec. III. The metasurface's TE noise is evaluated numerically using RCWA [36]. Figure 7 shows the linear relationship between the light phase $\Delta\varphi$ reflected by the metasurface and the parameter $\delta = \alpha\Delta T$. The slope of the line is the coefficient K_{TE}:

$$K_{\mathrm{TE}} = 5.21. \tag{A4}$$

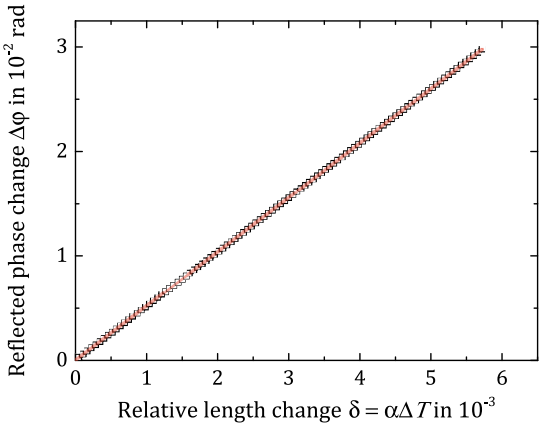

FIG. 7. Reflected light phase in dependence of different relative length changes. The values are obtained numerically using RCWA. Red denotes the linear line fit.

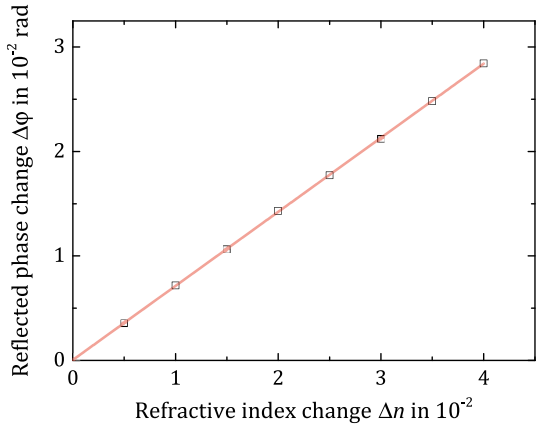

FIG. 8. Reflected light phase versus change of the refractive index of the metasurface material (silicon). The values are obtained numerically with RCWA. Red denotes the linear line fit.

3. Thermorefractive noise

Substrate and coating TR noise are evaluated analytically following Sec. III. The parameter for the determination of the metasurface's TR noise, K_{TR}, is the slope of the plot in Fig. 8:

$$K_{\mathrm{TR}} = 0.71. \tag{A5}$$

APPENDIX B: TABLES

TABLE II. Design parameters of the end mirrors of the Einstein Telescope low-frequency detector [14].

Parameter	Value (cm)
Mirror diameter d	50
Mirror thickness h	50
Gaussian beam radius r_0	6.36

TABLE III. Parameters of the single-crystalline silicon cavity for the stabilization of laser light at a frequency of 1.55 μm [25].

Parameter	Value
Cavity length L	210 mm
Central bore diameter $2a$	5 mm
Mirror diameter d	12.7 mm
Mirror thickness h	5 mm
Gaussian beam radius r_0	483 μm

TABLE IV. General parameters for the noise computations of the meta-etalon mirror.

Parameter	Value
Wavelength	1550 nm
Polarization	TEM_{00}
Metasurface material	c-Si
Metasurface refractive index n_g	3.48
Metasurface period Λ	950 nm
Metasurface ridge width W	298 nm
Metasurface ridge height H	175 nm
Metasurface residual transmission t_1	<0.7%, <0.1%, <0.01%
Substrate material	SiO_2
Substrate refractive index n_2	1.45
Coating composition	$18\lambda/4$ doublets of SiO_2/Ta_2O_5
Coating residual transmission t_2	6 ppm

TABLE V. Material properties of the meta-etalon components at room temperature [21,23].

Parameter	Silicon	Substrate	Ta_2O_5 layer	SiO_2 layer
β (1/K)	1.8×10^{-4}	8×10^{-6}	1.4×10^{-5}	8×10^{-6}
α (1/K)	2.62×10^{-6}	5.1×10^{-7}	3.6×10^{-6}	5.1×10^{-7}
ρ (kg/m^3)	2331	2202	6850	2202
Y (Pa)	130×10^9	72×10^9	140×10^9	72×10^9
ν	0.28	0.17	0.23	0.17
κ [W/(K m)]	148	1.38	33	1.38
C [J/(K kg)]	713	746	306	746
Φ	5×10^{-5}	4×10^{-10}	2×10^{-4}	4×10^{-5}
n	3.48	1.45	2.06	1.45

TABLE VI. Material properties of the meta-etalon components at 124 K [42].

Parameter	Silicon	Substrate	Ta_2O_5 layer	SiO_2 layer
β (1/K)	9×10^{-5}	4.2×10^{-6}	1.4×10^{-5}	4.2×10^{-6}
α (1/K)	≈ 0	-4.8×10^{-7}	3.6×10^{-6}	-4.8×10^{-7}
ρ (kg/m^3)	2331	2203	6850	2202
Y (Pa)	130×10^9	72×10^9	140×10^9	72×10^9
ν	0.28	0.16	0.23	0.16
κ [W/(K m)]	638	0.804	33	0.804
C [J/(K kg)]	328	339	306	339
Φ	5×10^{-6}	10^{-7}	2×10^{-4}	4×10^{-5}
n	3.48	1.45	2.06	1.45

[1] G. M. Harry *et al.* (LIGO Scientific Collaboration), Classical Quantum Gravity **27**, 084006 (2010).
[2] F. Acernese, M. Agathos, K. Agatsuma, D. Aisa, N. Allemandou, A. Allocca, J. Amarni, P. Astone, G. Balestri *et al.*, Classical Quantum Gravity **32**, 024001 (2015).
[3] K. Somiya, Classical Quantum Gravity **29**, 124007 (2012).
[4] T. Kessler, C. Hagemann, C. Grebing, T. Legero, U. Sterr, F. Riehle, M. Martin, L. Chen, and J. Ye, Nat. Photonics **6**, 687 (2012).
[5] H. Audley, S. Babak, J. Baker, E. Barausse, P. Bender, E. Berti, P. Binetruy, M. Born, D. Bortoluzzi, J. Camp *et al.*, arXiv:1702.00786.
[6] G. M. Harry, A. M. Gretarsson, P. R. Saulson, S. E. Kittelberger, S. D. Penn, W. J. Startin, S. Rowan, M. M. Fejer, D. Crooks, G. Cagnoli *et al.*, Classical Quantum Gravity **19**, 897 (2002).
[7] M. Principe, I. M. Pinto, V. Pierro, R. DeSalvo, I. Taurasi, A. E. Villar, E. D. Black, K. G. Libbrecht, C. Michel, N. Morgado *et al.*, Phys. Rev. D **91**, 022005 (2015).
[8] M. Granata, E. Saracco, N. Morgado, A. Cajgfinger, G. Cagnoli, J. Degallaix, V. Dolique, D. Forest, C. Franc, J. Michel, L. Pinard *et al.*, Phys. Rev. D **93**, 012007 (2016).
[9] T. Metcalf, X. Liu, and M. Abernathy, Plasma damage to silicon resonators measured by internal friction, Bulletin of the American Physical Society (2018).
[10] G. D. Cole, W. Zhang, M. J. Martin, J. Ye, and M. Aspelmeyer, Nat. Photonics **7**, 644 (2013).
[11] G. D. Cole, W. Zhang, B. J. Bjork, D. Follman, P. Heu, C. Deutsch, L. Sonderhouse, J. Robinson, C. Franz, A. Alexandrovski *et al.*, Optica **3**, 647 (2016).
[12] A. Cumming, K. Craig, I. Martin, R. Bassiri, L. Cunningham, M. Fejer, J. Harris, K. Haughian, D. Heinert, B. Lantz *et al.*, Classical Quantum Gravity **32**, 035002 (2015).
[13] A. Lin, R. Bassiri, S. Omar, A. S. Markosyan, B. Lantz, R. Route, J. S. Byer, R. L. and Harris, and M. M. Fejer, Opt. Mater. Express **5**, 1890 (2015).
[14] M. Abernathy, F. Acernese, P. Ajith, B. Allen, P. Amaro-Seoane, N. Andersson, S. Aoudia, P. Astone, B. Krishnan, L. Barack *et al.*, *Einstein Gravitational Wave Telescope Conceptual Design Study* (EGO, Cascina, Pisa, Italy, 2011).
[15] F. Acernese, M. Agathos, K. Agatsuma, D. Aisa, N. Allemandou, A. Allocca, J. Amarni, P. Astone, G. Balestri, G. Ballardin *et al.*, Classical Quantum Gravity **32**, 024001 (2015).
[16] P. Lalanne, J. Hugonin, and P. Chavel, J. Lightwave Technol. **24**, 2442 (2006).
[17] V. Karagodsky, F. G. Sedgwick, and C. J. Chang-Hasnain, Opt. Express **18**, 16973 (2010).
[18] F. Brückner, D. Friedrich, T. Clausnitzer, M. Britzger, O. Burmeister, K. Danzmann, E.-B. Kley, A. Tünnermann, and R. Schnabel, Phys. Rev. Lett. **104**, 163903 (2010).
[19] S. Kroker, T. Käsebier, E.-B. Kley, and A. Tünnermann, Opt. Lett. **38**, 3336 (2013).
[20] D. Friedrich, B. Barr, F. Brückner, S. Hild, J. Nelson, J. Macarthur, B. Plissi, M. Edgar, B. Huttner, S. H. Sorazu, S. Kroker *et al.*, Opt. Express **19**, 14955 (2011).
[21] D. Heinert, S. Kroker, D. Friedrich, S. Hild, E.-B. Kley, S. Leavey, I. W. Martin, R. Nawrodt, A. Tünnermann, S. P. Vyatchanin *et al.*, Phys. Rev. D **88**, 042001 (2013).
[22] S. Kroker, J. Dickmann, C. Rojas Hurtado, D. Heinert, R. Nawrodt, Y. Levin, and S. Vyatchanin, Phys. Rev. D **96**, 022002 (2017).
[23] J. Dickmann, C. R. Hurtado, R. Nawrodt, and S. Kroker, Phys. Lett. A **382**, 2275 (2018).
[24] M. Born and E. Wolf, *Principles of Optics: Electromagnetic Theory of Propagation, Interference and Diffraction of Light*, 7th ed. (Cambridge University Press, Cambridge, England, 1999).
[25] D. Matei, T. Legero, S. Häfner, C. Grebing, R. Weyrich, W. Zhang, L. Sonderhouse, J. Robinson, J. Ye, F. Riehle *et al.*, Phys. Rev. Lett. **118**, 263202 (2017).
[26] M. Evans, S. Ballmer, M. Fejer, P. Fritschel, G. Harry, and G. Ogin, Phys. Rev. D **78**, 102003 (2008).
[27] S. T. Dawkins, J. J. McFerran, and A. N. Luiten, IEEE Trans. Ultrason. Ferroelectr. Freq. Control **54**, 918 (2007).
[28] M. Tugolukov, Y. Levin, and S. Vyatchanin, Phys. Lett. A **382**, 2181 (2018).
[29] Y. Levin, Phys. Rev. D **57**, 659 (1998).
[30] K. Somiya, A. G. Gurkovsky, D. Heinert, S. Hild, R. Nawrodt, and S. P. Vyatchanin, Phys. Lett. A **375**, 1363 (2011).
[31] A. G. Gurkovsky, D. Heinert, S. Hild, R. Nawrodt, K. Somiya, S. P. Vyatchanin, and H. Wittel, Phys. Lett. A **375**, 4147 (2011).
[32] COMSOL Multiphysics v 5.2, www.comsol.com.
[33] F. Bondu, P. Hello, and J.-Y. Vinet, Phys. Lett. A **246**, 227 (1998).
[34] N. Nakagawa, A. Gretarsson, E. Gustafson, and M. Fejer, Phys. Rev. D **65**, 102001 (2002).
[35] Y. T. Liu and K. S. Thorne, Phys. Rev. D **62**, 122002 (2000).
[36] M. Moharam and T. Gaylord, J. Opt. Soc. Am. **71**, 811 (1981).
[37] V. Braginsky and S. Vyatchanin, Phys. Lett. A **312**, 244 (2003).
[38] M. Wurm, J. Endres, J. Probst, M. Schoengen, A. Diener, and B. Bodermann, Opt. Express **25**, 2460 (2017).
[39] J. Degallaix, R. Flaminio, D. Forest, M. Granata, C. Michel, L. Pinard, T. Bertrand, and G. Cagnoli, Opt. Lett. **38**, 2047 (2013).
[40] A. Khalaidovski, J. Steinlechner, and R. Schnabel, Classical Quantum Gravity **30**, 165001 (2013).
[41] S. Kroker, T. Käsebier, S. Steiner, E.-B. Kley, and A. Tünnermann, Appl. Phys. Lett. **102**, 161111 (2013).
[42] D. Heinert, C. Schwarz, G. Hofmann, J. Komma, and R. Nawrodt, Database of bulk material properties, https://tds.virgo-gw.eu/ql/?c=10033.